In(Ga)As/GaAs(001) quantum dot molecules probed by nanofocus high resolution x-ray diffraction with 100 nm resolution

M. Dubslaff,[1] M. Hanke,[1,a)] M. Burghammer,[2] S. Schöder,[2] R. Hoppe,[3] C. G. Schroer,[3] Yu. I. Mazur,[4] Zh. M. Wang,[4] J. H. Lee,[4,5] and G. J. Salamo[4]
[1]*Paul-Drude-Institut für Festkörperelektronik, Hausvogteiplatz 5-7, D-10117 Berlin, Germany*
[2]*European Synchrotron Radiation Facility, BP 220, F-38043 Grenoble Cedex, France*
[3]*Institut für Strukturphysik, Technische Universität Dresden, Zellescher Weg 16, D-01069 Dresden, Germany*
[4]*Department of Physics, University of Arkansas, Fayetteville, Arkansas 72701, USA*
[5]*School of Electronics and Information, Kwangwoon University, Nowon-gu, Seoul 139-701, South Korea*

(Received 8 March 2011; accepted 4 May 2011; published online 24 May 2011)

In(Ga)As quantum dots, which laterally self-assemble into quantum dot molecules, have been studied by scanning x-ray nanodiffraction, finite element calculations and subsequent kinematical diffraction simulations. X-ray beam sizes of 100 nm enable small scattering volumes comparable to the object size at extremely high local flux densities ($\approx 10^4$ photons nm^{-2} s^{-1}). By that bulk contributions to the scattering are effectively reduced. Area maps of various individual quantum dot molecules have been measured, whereas the diffraction patterns therein reveal spatially resolved information about the inter quantum dot position correlation function. © *2011 American Institute of Physics*. [doi:10.1063/1.3593960]

Charge carriers within low-dimensional semiconductor structures close or smaller than the deBroglie wavelength (about 25 nm for electrons in InAs) show confined wave functions, whereas quantum dots (QDs) represent the highest degree of confinement in all three dimensions. Throughout the last decade they have been extensively studied and can be used nowadays in devices like single electron transistors,[1,2] QD memories,[3] single photon sources[4,5] (i.e., for quantum cryptography), QD photodiodes,[6] and lasers.[7,8] If several QDs assemble very close together an overlap of the wave functions becomes possible, which enables carrier tunneling from one QD to another. By analogy to chemistry, where molecules consist of atoms with confined electrons, hierarchical QD ensembles are called QD molecules (QDMs). Their electronic properties depend in particular on the size, shape, chemical composition and thereby elastic strain, positional correlation and orientation of the QDs. For instance energy levels, the influence of thermal fluctuations and, in case of optical applications as laser sources, optical gain and wavelength are strongly influenced by the size and shape of the QDs.

In order to control the properties and to reveal some fundamentals behind the growth of self-assembled semiconductor nanostructures high resolution x-ray diffraction (HRXRD) serves as a well established technique. Since synchrotron radiation sources provide highly brilliant and nowadays even highly focused hard x-rays, *nanofocus* HRXRD (nHRXRD) is an upcoming analytical tool.[9,10] nHRXRD can be applied to obtain information about positional correlation, geometrical, and chemical properties.[11] It combines the inherently high resolution in reciprocal space of HRXRD with a sub-micrometer spatial resolution (due to the focus size) which together enables a probe of individual structures. Here, we present an experiment using a 100 nm x-ray spot full width at half maximum (FWHM) on In(Ga)As/GaAs QDMs.

The In(Ga)As/GaAs(001) QDMs used for the recent study are shown in Fig. 1. They were grown by molecular beam epitaxy in a template-free, self-organizing way which combines droplet epitaxy (homoepitaxy) and Stranski–Krastanov growth mode (heteroepitaxy).[12,13] By varying the growth conditions the QD and QDM density can be controlled. At first a GaAs droplet is formed by depositing three monolayers of Ga at the GaAs(001) substrate at a surface temperature of 500 °C which leads to liquid metal Ga droplets. These droplets finally crystallize to GaAs mounds by exposing them to As_4 flux. To reduce the anisotropic surface diffusion and thus preserve the shape of the originating Ga droplets, the crystallization has been performed at a lower surface temperature of 150 °C (i.e., an increased crystallation temperature would have lead to ringlike mounds as presented in[14]). The resulting homoepitaxial GaAs mounds are free of elastic strain and can be used as templates for the following Stranski–Krastanov growth of In(Ga)As QDs, which nucleate close to the mounds. Depending on the de-

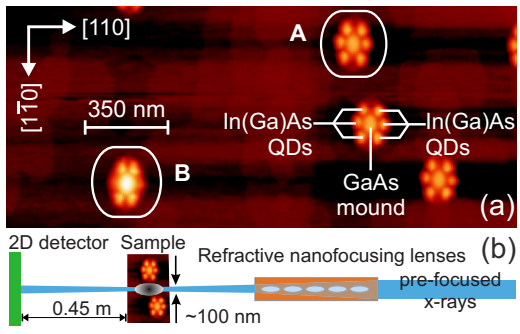

FIG. 1. (Color online) (a) Atomic force micrograph of In(Ga)As/GaAs(001) QDMs. Type A consists of an inner GaAs mound surrounded by six In(Ga)As QDs while type B depicts an intermediate growth stage of a QDM. Scheme of the experimental setup (b) for nHRXRD. Due to the x-ray's footprint the spot size deteriorates in [110] direction to about 350 nm.

a)Electronic mail: hanke@pdi-berlin.de.

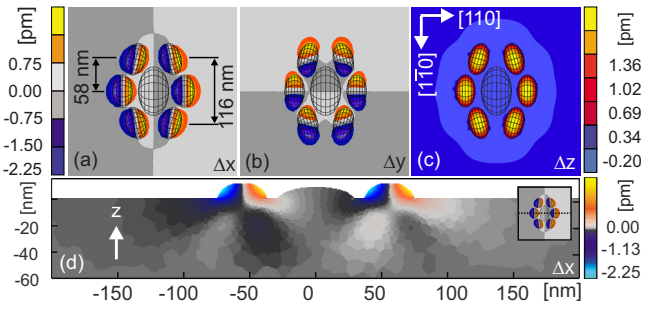

FIG. 2. (Color online) Finite element calculations on elastic strain caused by heteroepitaxial lattice mismatch, in-plane (a) and (b) and out-of-plane (c). (d) Shows a slice through the three-dimensional data of (a) in [110] direction. The QDs contain homogeneous indium content.

posited amount of InAs monolayers bimolecules, QDMs with four and eventually six In(Ga)As QDs are formed. Approximately 80% are hexapodlike as shown in Fig. 1(a) while the remaining QDMs nucleate as quadruplets around the GaAs mounds.

The local arrangement of QDs into hexapodlike QDMs already indicates that elastic strain may play a crucial role during the self-formation and assembling. Obviously the mounds serve as ideal nucleation spots. For the final morphology, we have calculated the three-dimensional distribution of elastic strain (within the QDMs and the surrounding GaAs matrix) by numerical finite element method (FEM). Figure 2 gives the in-plane [(a) and (b)] and out-of-plane (c) components of the displacement field. Due to different azimuthal QD orientations and the elastic anisotropy the resulting strain tensor appears to be inequivalent for the individual QDs. We have to mention that elastic strain is also present in the substrate around and especially directly below the QDM (d), which emphasizes the intermediating character of the substrate for the formation of QDMs. In particular, this part of the deformation field serves as contrast mechanism during nHRXRD.

Standard x-ray techniques (using millimeter sized x-ray spots) provide an ensemble information. In order to probe first the average morphology of the QDMs (shape, size, and chemical composition) we have performed grazing incidence diffraction (GID) using an x-ray energy of 8 keV (beamline ID10B, European Synchrotron Radiation Facility ESRF, Grenoble). Figure 3(a) shows the diffusely scattered intensity

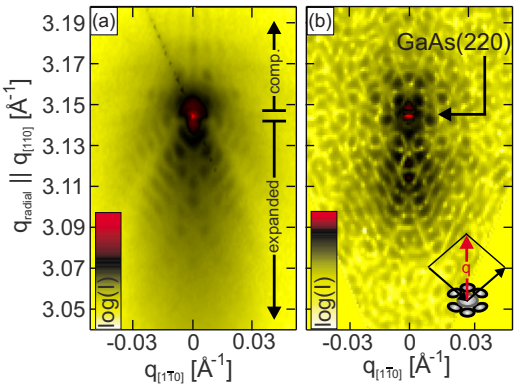

FIG. 3. (Color online) Measured (a) and simulated (b) diffuse intensity near the GaAs(220) in- plane reciprocal lattice point. The intensity distribution has been measured in GID averaging over a large ensemble of objects. A scheme of this geometry is shown as inset in (b).

near the GaAs(220) reciprocal lattice point. This distribution is caused first by the shape of the QDMs and second the in-plane strain component of the elastic strain tensor. Smaller values of $q_{[110]}$ (along the radial direction) generally correspond to laterally *expanded* regions which coincides with the QD apex. Whereas intensity at larger $q_{[110]}$, in particular beyond the GaAs(220) substrate reflection at 3.15 Å^{-1}, are caused by laterally *compressed* areas in the substrate, see Fig. 2(d). An improved simulation (b) based on various FEM morphologies and concentration profiles clearly confirm that the elongation of the (220) reflection in [110] direction can be ascribed to the elastic relaxation within the QDMs. Comparing the measured intensity with systematic simulations yield an averaged indium content of about $(30 \pm 5)\%$ within the surrounding In(Ga)As QDs.

HRXRD using synchrotron radiation (not shown here) did not reveal any signature of the QDMs in the diffuse scattering. The principal reason for this may be the very poor ratio of nanostructures and substrate material. Here, the most part of the millimeter-sized beam spot (95%) illuminates just the plane surface and thus prevents a measure of low density QDMs in this geometry. To overcome this drawback and the ensemble averaging itself, we have performed nHRXRD. There are only a very few beamlines which offer x-rays with suitable characteristics in terms of brilliance, collimation and energy resolution. The respective experiment has been realized at the dedicated nanofocus facility at beamline ID13 (ESRF). By stacks of refractive nanofocusing lenses[15] the x-ray beam can be focused down to a size of 100 nm at an energy of 15.25 keV and a spectral width $\Delta E/E$ of 10^{-4}. A spot intensity of 10^8 cps yields the extremely high flux density of 10^4 counts nm^{-2} s^{-1}.

As illustrated in Fig. 1 the nanofocused x-ray beam illuminates the sample along [110]. At a Bragg angle $\Theta_{Bragg}^{GaAs(004)}$ of 16.5° the spot will be smeared out due to its footprint to about 350 nm, whereas along [1$\bar{1}$0] the original size of 100 nm is preserved. The FWHMs have been measured by a knife edge scan. We have scanned the surface by translating the sample in discrete steps of 200 and 100 nm along [110] and [1$\bar{1}$0], while recording reciprocal space maps (RSMs) with a high sensitivity two-dimensional (2D) pixel detector (MAXIPIX).

Composing all RSMs together yields *spatially resolved* information in reciprocal space. For a better view just a selection of it is plotted in Fig. 4(a). The framed area therein highlights 2×4 RSMs which fit very well to the dimensions of one single QDM. However, the diffraction patterns are in some cases still visible even if the spot has been moved up to 7 steps along [110] (footprint direction) or 3 steps in [1$\bar{1}$0] direction. Here, we cannot exclude, that more than one QDM has been illuminated at the same time with the actually 100 nm by 350 nm spot since the mean density of the randomly placed QDMs amounts to $2.5/\mu m^2$ which is in agreement to the density calculated by counting the QDMs apparently hit in the area map [Fig. 4(a) shows a part of this area map only].

The measurements in Fig. 4 show a remarkably low intensity of only a few cps (captured with an exposure time of 60 s). To get better statistics from the rather weak diffuse intensities, Figs. 4(a) and 4(b) has been generated by averaging over 17 RSMs of one specific QDM [at the same beam

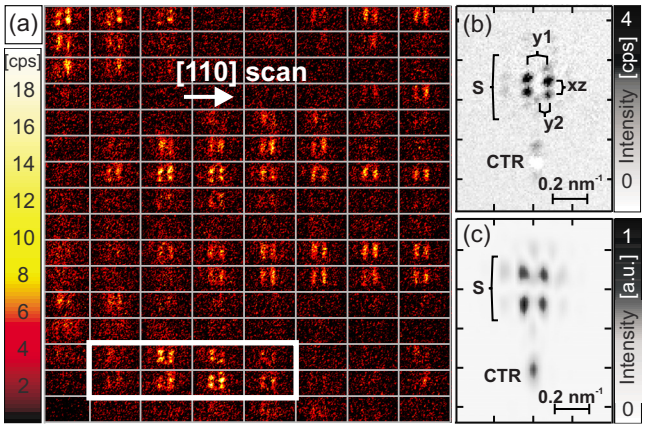

FIG. 4. (Color online) Array of 8×16 RSMs from adjacent x-ray spot positions along [110] and $[1\bar{1}0]$ captured close to the GaAs(004) reflection. The array represents an area map of the sample surface. (b) RSM of one specific QDM [at position of the highlighted area in (a)]. (c) Kinematical scattering simulation.

spot position like highlighted in Fig. 4(a)]. An average background image of RSMs without diffuse diffraction spots at the same position in reciprocal space has been subtracted. As one would expect, the intensity at the position of the GaAs(001) crystal truncation rod (CTR) is reduced if the beam hits a QDM and thus, due to the subtracted background, appears as a white spot in Fig. 4(b).

Please keep in mind that the diffuse diffraction patterns appear near the substrate reflection. In all simulations the In(Ga)As reflection (not shown here) is clearly visible at lower q_{radial} but could not be seen in the measurement because of intensity reasons. The diffuse part around the GaAs(004) peak consists of well separated spots with distances y_1, y_2, and xz, Fig. 4. These basically reflect the Fourier transform of the positional correlation function of the individual QDs within the QDM. Their separation in reciprocal space correspond to the inter-QD distance in real space via $\Delta\mathbf{x}=2\pi/\Delta\mathbf{q}$. Since the horizontal axis in Figs. 4(b) and 4(c) runs parallel to $[1\bar{1}0]$, $y_{1,2}$ correspond to real space lengths in this in-plane direction, namely along the longer axis of the QDM. They amount to $y_1=0.108$ nm^{-1} and $y_2=0.055$ nm^{-1} in the nHRXRD measurement and simulation (c) which, on the other hand, fits well to respective atomic force microscopy (AFM) results ($y_1^{\mathrm{AFM}}=58$ nm and $y_2^{\mathrm{AFM}}=116$ nm).

Each RSM detected by the 2D detector represents a tilted (and slightly curved) slice through the reciprocal space. Thus, the vertical axis in the RSM (distances xz) contains information about the in-plane [110] direction and along the surface normal [001]. However, the model for our simulations has still to be refined since xz in measurement (0.06 nm^{-1}) and simulation (0.15 nm^{-1}) are at variance. As it can be seen in Fig. 4(a) the spots sometimes smear out to lines in direction of xz but at the same time still reveal $y_1=0.108$ nm^{-1} and $y_2=0.055$ nm^{-1}. Further simulations for QDMs with four surrounding In(Ga)As QDs, comparable to QDM in Fig. 1(b), also show spots that are not separated in this direction which may indicate that the intensity distribution in this direction is very sensitive to the centered outer In(Ga)As dots.

We acknowledge the German Research Foundation (DFG) for financial support, Project No. HA3495/6-1 and the European Synchrotron Radiation Facility for financial and technical support during experiments SI-1870 and SI-1972.

[1]S. J. Angus, A. J. Ferguson, A. S. Dzurak, and R. G. Clark, Appl. Phys. Lett. **92**, 112103 (2008).
[2]O. Klochan, J. C. H. Chen, A. P. Micolich, A. R. Hamilton, K. Muraki, and Y. Hirayama, Appl. Phys. Lett. **96**, 092103 (2010).
[3]M. Geller, A. Marent, T. Nowozin, D. Bimberg, N. Akçay, and N. Öncan, Appl. Phys. Lett. **92**, 092108 (2008).
[4]M. B. Ward, O. Z. Karimov, D. C. Unitt, Z. L. Yuan, P. See, D. G. Gevaux, A. J. Shields, P. Atkinson, and D. A. Ritchie, Appl. Phys. Lett. **86**, 201111 (2005).
[5]O. D. D. Couto, S. Lazić, F. Iikawa, J. A. H. Stotz, U. Jahn, R. Hey, and P. V. Santos, Nat. Photonics **3**, 645 (2009).
[6]A. Zrenner, E. Beham, S. Stufler, F. Findeis, M. Bichler, and G. Abstreiter, Nature (London) **418**, 612 (2002).
[7]D. Bimberg, N. N. Ledentsov, M. Grundmann, N. Kirstaedter, O. G. Schmidt, M. H. Mao, V. M. Ustinov, A. Y. Egorov, A. E. Zhukov, P. S. Kopev, Z. I. Alferov, S. S. Ruvimov, U. Gösele, and J. Heydenreich, Phys. Status Solidi B **194**, 159 (1996).
[8]D. L. Huffaker, G. Park, Z. Zou, O. B. Shchekin, and D. G. Deppe, Appl. Phys. Lett. **73**, 2564 (1998).
[9]Y. Xiao, Z. Cai, and B. Lai, Nanotechnology **16**, 1754 (2005).
[10]M. Hanke, M. Dubslaff, M. Schmidbauer, T. Boeck, S. Schöder, M. Burghammer, C. Riekel, J. Patommel, and C. G. Schroer, Appl. Phys. Lett. **92**, 193109 (2008).
[11]M. Dubslaff, M. Hanke, S. Schöder, M. Burghammer, T. Boeck, and J. Patommel, Appl. Phys. Lett. **96**, 133107 (2010).
[12]J. H. Lee, Z. M. Wang, N. W. Strom, Y. I. Mazur, and G. J. Salamo, Appl. Phys. Lett. **89**, 202101 (2006).
[13]Z. M. Wang, B. Liang, K. A. Sablon, J. H. Lee, Y. I. Mazur, N. W. Strom, and G. J. Salamo, Small **3**, 235 (2007).
[14]M. Hanke, Y. I. Mazur, J. E. Marega, Z. Y. AbuWaar, G. J. Salamo, P. Schäfer, and M. Schmidbauer, Appl. Phys. Lett. **91**, 043103 (2007).
[15]C. G. Schroer, P. Boye, J. M. Feldkamp, J. Patommel, A. Schropp, and A. Schwab, Phys. Rev. Lett. **101**, 090801 (2008).